Available online at www.sciencedirect.com
SCIENCE DIRECT
ELSEVIER
Journal of the European Ceramic Society 26 (2006) 2677–2684
ECERS
www.elsevier.com/locate/jeurceramsoc

Prediction of crack propagation and fracture in residually stressed glass as a function of the stress profile and flaw size distribution

Matthew B. Abrams [1], David J. Green *

Department of Materials Science and Engineering, 230 Steidle Building, The Pennsylvania State University, State College, PA 16802, USA

Received 22 February 2005; received in revised form 23 June 2005; accepted 16 July 2005
Available online 16 September 2005

Abstract

Engineered stress profile (ESP) glasses are noted for narrow strength distributions and the potential for stable growth of multiple surface cracks under applied tensile stress. This behavior depends on the interaction of the surface flaw size distribution with the residual stress profile in the material. In this work, several surface preparation methods were used to produce a range of flaw size distributions in soda lime silica glass specimens. Two ion exchange processes were then performed on these specimens to produce ESP glass. For each condition, crack growth behavior and fracture strength were experimentally observed. Residual stress profiles resulting from each ion exchange process were measured with an optical technique. These stress profiles were used to calculate stress intensity factors as a function of crack geometry, using a weight function method. Crack growth and fracture strength predictions based on these stress intensity factors were compared to experimental data, resulting in good agreement in most cases.

Keywords: Ion exchange; Mechanical properties; Fracture; Toughness and toughening; Glass

1. Introduction

Glass articles commonly fail from surface flaws under tension. Thus, residual surface compression is used to increase fracture strength. These residual surface stresses are normally introduced by ion exchange or thermal tempering. Ion exchange can produce higher compressive stresses resulting in increased strength, but typical exchange depths are relatively shallow (<200 μm).[1–3] Flaws similar in size to this compressive region usually limit the desired improvement in strength and increase the strength dispersion.[4,5]

This effect can be modified by changing the shape of the residual stress profile. A review paper by Schaeffer[6] suggests that placing the maximum compressive stress beneath the surface produces a "stress barrier" which arrests crack growth. Tandon and Green[7,8] analyzed conditions for crack arrest and stabilization for parabolic stress distributions. A subsurface residual stress maximum was predicted to result in a defined region of stable crack growth. If surface flaws were limited to this stable growth region then strength variability would be significantly reduced. Later work by Green[9] quantified the effects of a parabolic residual stress layer on fracture strength and defined the limiting conditions for stable surface crack growth.

Experimental work[10,11] has produced glasses which exhibit these stable crack growth behaviors and associated narrow strength distributions using two-step ion exchange processes applied to soda alumina silica glass. Similar behavior has been seen for soda lime silica (SLS) float glasses for two-step[12,13] and variable temperature[14] ion exchange processes. The resulting materials are termed engineered stress profile (ESP) glasses.

In previous mathematical analyses of the fracture behavior of ESP glasses, little attention has been paid to the growth process of the stable surface cracks. Specifically, near-equiaxial

* Corresponding author. Tel.: +1 814 863 2011; fax: +1 814 865 0016.
E-mail addresses: matthew.abrams@gmail.com (M.B. Abrams), djg7@psu.edu (D.J. Green).
[1] Present address: 1304 Liriope Ct. # 202, Belcamp, MD 21017, USA. Tel.: +1 443 910 5026.

0955-2219/$ – see front matter © 2005 Elsevier Ltd. All rights reserved.
doi:10.1016/j.jeurceramsoc.2005.07.065

flaws have been observed to grow into through-thickness surface cracks, propagating preferentially across the surface without penetrating the compressive stress layer.[11] The prior theoretical models of the fracture process have, however, assumed the flaws to begin as through-thickness, with no change in geometry as the crack propagates.

An extended theory has recently been put forward to describe the evolution of low-aspect ratio semi-elliptical cracks in these materials as a function of flaw size. This approach more fully explains and predicts the observed fracture behavior.[15] The primary objective of the current work is to study the fracture behavior of ESP glasses with different surface flaw sizes and to compare the fracture behavior with the extended theory.

2. Experimental procedure

2.1. Preparation of glass specimens

A commercial SLS float glass was used in these experiments (Starphire, PPG Industries, Pittsburgh, PA). The composition of the glass was 72 mol% SiO_2, 13.9% Na_2O, 11.0% CaO, 0.7% Al_2O_3, 0.1% SrO, 0.1% MgO, 2% other,[13] with a strain point temperature of ~475 °C.[16]

The as-received glass was cut into 50 mm × 10 mm × 3.2 mm specimens, using a diamond-wafering blade. The specimens were examined with a polariscope to ensure that no pre-existing residual stresses were present which might interfere with the ion exchange processing. Three polishing techniques, as described in Table 1, were chosen to smooth the chamfered specimen edges, in order to produce three distinct flaw size distributions. No re-annealing was performed after polishing, in order to retain a sharp, relatively pristine flaw geometry. Two ion exchange processes were then conducted, based on prior work[12,13]: a single-step exchange in molten KNO_3 at 450 °C for 48 h, and a two-step exchange which added a subsequent mixed salt bath (1.68 KNO_3:1 $NaNO_3$ molar ratio) at a temperature of 400 °C for 30 min.

Groups of 20 specimens were selected representing each surface preparation and each ion exchange condition. These specimens were fractured in four-point-bend configuration with an outer span of 40 mm and an inner span of 20 mm, at a strain rate of $\sim 3 \times 10^{-3}\ s^{-1}$. Tests were performed in ambient atmosphere, and samples were taped to retain fragments. The measured fracture strengths of the glass prior to ion exchange were used to predict size distributions for the largest flaws present in the material, using the fracture toughness equation

$$c = \left(\frac{T}{\sigma_F Y}\right)^2 \quad (1)$$

where T is the known fracture toughness of the material, 0.7 MPa $m^{1/2}$.[16] σ_F is the measured fracture strength, Y is a geometric factor based on crack geometry, and c is the crack depth. Crack growth is assumed to be exclusively Mode I. Choice of a value for Y is significant. In this research, two limiting cases are discussed, a semi-circular surface crack with $Y = 2.24/\pi^{1/2}$, and a through-thickness surface crack with $Y = 1.12\pi^{1/2}$. In this work, a group of the specimens is subjected to ion exchange after machining. It is realized that this treatment could change flaw sizes and crack tip geometry. An attempt could be made to approximate this effect in the non-exchanged specimens by an annealing treatment, but this would still not include the effect of molten salt during ion exchange. It was decided, therefore, to forego any heat treatments on the machined glass specimens.

2.2. Observation of multiple surface cracking behavior

Additional specimens representing each ion exchange process were loaded in four-point bending to a stress below the final fracture stress, then immediately unloaded. The tensile surface of each specimen was examined using an optical microscope. The visible surface trace length was measured for all surface cracks, and the number of cracks longer than 100 μm was recorded. This threshold length was chosen to avoid confusing the extended surface cracks caused by loading with pre-existing flaws in the glass. The experiment was then repeated at successively higher applied stresses. The dimensions of these specimens were the same as those used in the strength testing.

2.3. Stress profile measurement

The residual stresses induced in the glass by ion exchange were measured using optical birefringence and progressive etching.[17] As-received plates were cut to dimensions of 100 mm × 50 mm, and polished to improve optical transmission, then processed in the ion exchange salt baths, producing a compressive surface stress and a compensating internal tensile stress.

Table 1
Strength of untreated glass and flaw size estimation after various surface preparations

Surface finish	Polishing media used in final step of surface preparation	Average fracture strength (MPa)	Standard deviation (MPa)	Calculated semi-circular flaw sizes (μm)	Calculated through-thickness flaw sizes (μm)
Coarse	12.5–17 μm SiC[a]	98.4	7.5	24.3–46.5	9.9–18.9
Medium	1.5–5 μm SiC[a]	113.7	11.7	17.9–38.8	7.3–15.8
Fine	0.3 μm Al_2O_3	119.5	6.8	17.4–25.7	7.1–10.4

[a] Particle diameter size range, according to manufacturer's data.[24]

The tensile stresses in the interior of each specimen were measured using conventional optical retardation techniques. The glass surface was then etched by immersion in a 5% solution of hydrofluoric acid. The stress measurement was repeated, and the change in the compensating internal tensile stress was used to calculate the average stress in the etched surface region. By repeating this process for successive etch steps, the residual stress profile resulting from each ion exchange process was evaluated, with a depth resolution of ~1 μm and an estimated accuracy of ±10% of the peak residual stress.[18]

2.4. Stress intensity factor calculations

The measured stress profiles for each ion exchange process were then used to produce stress intensity factor values for semi-elliptical cracks in the material, using a weight function method shown in Eq. (2).

$$K = \int_0^a \sigma(y) m(y, a, \alpha)\, \mathrm{d}y \tag{2}$$

where K is the stress intensity factor, y measures depth beneath the glass surface, a is the depth of the crack, and α is the crack aspect ratio, a/c. The stress distribution $\sigma(y)$ is equal to the sum of the applied stress (assumed to be tensile and approximately constant over the crack depth) and the residual stress profile. The weight function $m(y, a, \alpha)$ uses the first four terms of the polynomial forms given by Shen and Glinka.[19,20] These truncated solutions are not exact, but have been successfully verified in prior work[19–21] against finite element and specific analytical solutions for a range of crack geometries. A full description of the method is given in a recent paper.[15]

2.5. Prediction of multiple cracking behavior and fracture strength

The stress intensity factors produced by the weight function method were then used to predict the applied stress at which cracks of a given size and geometry are expected to propagate through the material. By calculating the stress intensity factor at the surface and at the deepest point of the crack, a distinction can be made between surface growth indicating multiple surface cracking behavior, and depthwise growth which can lead to fracture. The procedure is described in detail in prior work.[15,18]

The results of these calculations can be plotted as a contour map of the applied stresses needed to propagate a specific flaw depth and geometry in a material with a particular fracture toughness and residual stress profile. These maps can be combined with the flaw size data calculated from the experimentally measured strengths of the untreated glass. The result is a predicted fracture strength distribution for a glass with a given initial flaw distribution and residual stress profile. For the ESP glasses, the onset of multiple cracking can also be predicted.

3. Results

3.1. Fracture strength of ESP glasses

Fracture strengths for the untreated glass are shown in Table 1. As expected, the coarser surface preparations produced lower fracture strengths. Strength results for the ion-exchanged glasses are given in Fig. 1. The first exchange step increases the strength of the material for all surface preparations. Compared to the single step process, the second exchange step causes a reduction in strength, with a significant reduction in strength variability for the medium and fine surface preparations. Note that the strength of the single-step ion-exchanged glass varies significantly with surface finish, with much higher strength and much wider standard deviation for the fine surface finish. In contrast, the strength of the untreated glass shows a moderate dependence on surface finish and the strength of the two-step exchanged glass remains virtually constant. This insensitivity to surface flaw size and associated decreased strength variability for the two-step process is characteristic of ESP glasses. Included in Table 1 are the calculated flaw sizes as determined from Eq. (1). Cracks are estimated to be larger if they are assumed to be semi-circular rather than through-thickness.

3.2. Multiple cracking behavior

For the glasses subjected to the two-step process, multiple cracking was observed on the tensile surfaces of the bend specimens. This behavior was absent in the specimens subjected to the one-step process. This distinction is consistent with prior studies of ESP glasses.[10–13] Surface cracks progress from localized origins at the chamfered tensile surface corners, as shown in Fig. 2, to through-thickness geometry as shown in Fig. 3, with increasing stress.

The number of surface cracks also increases with increasing applied stress, as shown in Fig. 4. This increase suggests

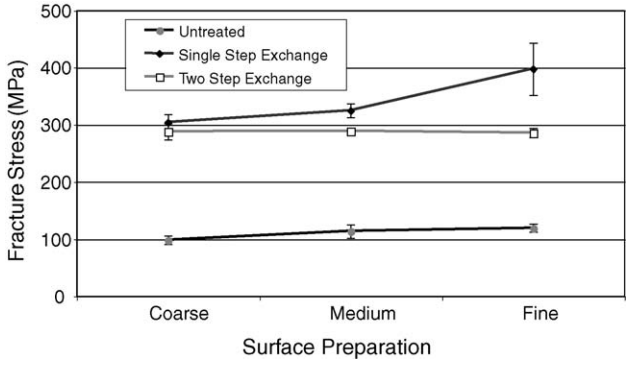

Fig. 1. Fracture strength of soda lime silica glass as a function of surface preparation and ion exchange processing.

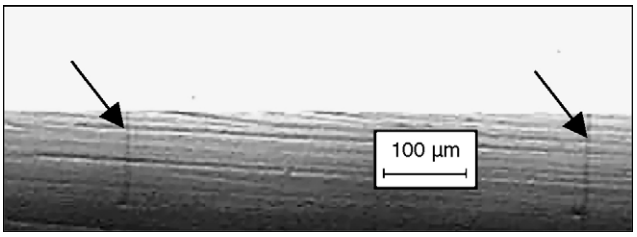

Fig. 2. Two-step ion-exchanged glass four-point-bend specimen at 150 MPa applied stress, with fine surface finish. Arrows indicate localized growth of surface cracks at edge of tensile surface.

Fig. 3. Through-thickness surface cracks across tensile surface of two-step ion-exchanged glass four-point-bend specimen at 210 MPa applied stress (fine surface finish).

that as the applied stress increases, a greater proportion of surface flaws within the material undergo stable growth. The distribution of cracks is distinctly non-uniform, with distances between adjacent cracks ranging from less than 20 to more than 200 μm. This variability seems to indicate an underlying uneven distribution of initiating flaws in the material. Fig. 5 plots the increase in stable surface crack density with increasing applied stress, averaging data for four specimens per condition. Only cracks of 100 μm or greater surface

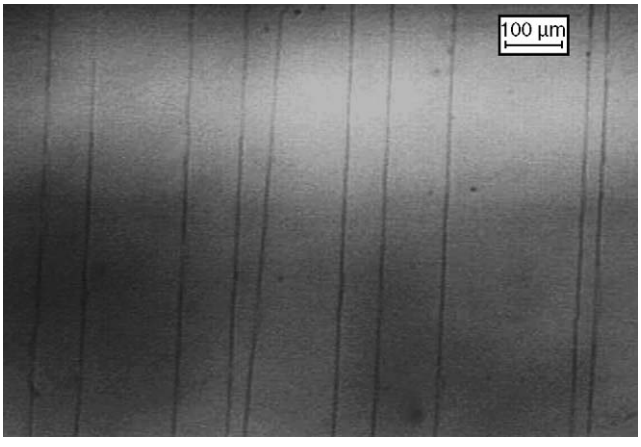

Fig. 4. Dense growth of multiple parallel surface cracks on tensile surface of two-step ion-exchanged glass four-point-bend specimen at 229 MPa applied stress (fine surface finish).

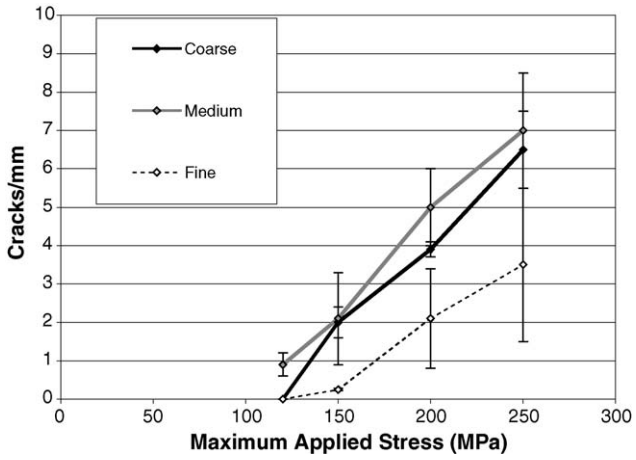

Fig. 5. Growth of multiple surface cracks on two-step ion-exchanged glass as a function of surface finish and applied stress.

length were considered, in order to avoid confusion with pre-existing flaws in the glass. Error bars indicate the relatively large variation between specimens. The data suggest that the fine surface finish reduces the number of stably growing surface flaws, compared to the medium and coarse surface finishes.

Analysis of multiple crack growth in these glasses is somewhat biased by the prevalence of cracks propagating from the corners of the four-point-bend specimens. This is expected, since the edges of the specimen must be cut and polished, producing machining flaws, while the tensile surface remains in relatively pristine condition. However, this flaw distribution may complicate later crack propagation calculations. The stress state along the edges of the specimen is different from that hypothesized for an infinite flat surface, due both to the presence of an additional free surface and the altered, three-dimensional stress profile caused by ion-exchange from both surfaces simultaneously. Thus, cracks approaching or emanating from the edges of the specimen will behave differently than those present on the flat tensile surfaces.

3.3. Stress profile data

Fig. 6 shows the measured stress profiles for both ion-exchanged glasses. The first exchange step produces a compressive stress layer that extends to ∼40 μm depth, with a maximum stress of −250 MPa. Note that the peak compressive stress is located beneath the surface of the material, since the near-surface region reaches maximum compressive stress first during the exchange process, and thus has more time for thermal relaxation. The short duration second exchange step removes potassium ions from the relaxed surface region, resulting in a tensile surface stress of ∼200 MPa. This effect decreases rapidly with depth, and the two profiles appear identical beyond 7 μm below the surface. This rapid change in the residual stress profile in the near surface region is the cause of the unusual fracture behavior seen in ESP glass, and the extent of the surface tensile layer exerts considerable

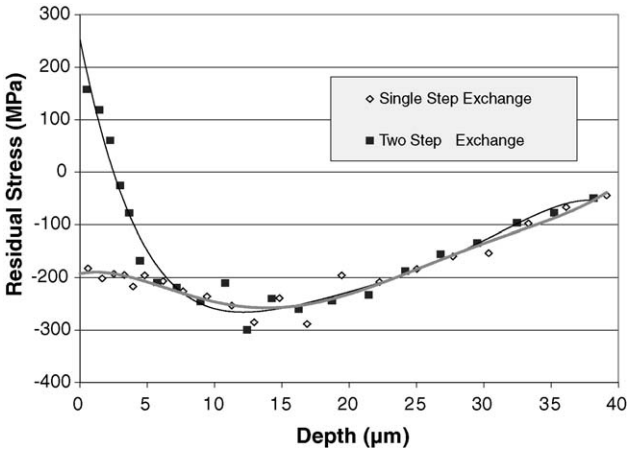

Fig. 6. Measured residual stress profiles for ion-exchanged glasses. Trend lines are 5th order polynomial curves as follows: Single step: $y = 0.0000478x^5 - 0.00511x^4 + 0.189x^3 - 2.48x^2 + 5.10x - 193$, Two step: $y = -0.000101x^5 + 0.0117x^4 - 0.529x^3 + 11.9x^2 - 128x + 252$. Depth x is in units of μm, residual stress y is in units of MPa.

control over crack propagation.[9–15,18] Fifth-order polynomial curves were fitted to the stress profile data by the least-squares method, and used as trend lines and for further stress intensity factor calculations.

3.4. Theoretical prediction of surface crack growth and fracture stress

Fig. 7 shows a crack propagation graph derived from stress intensity factor calculations for the two-step ion-exchanged ESP glass. Stable crack growth is mapped as a function of

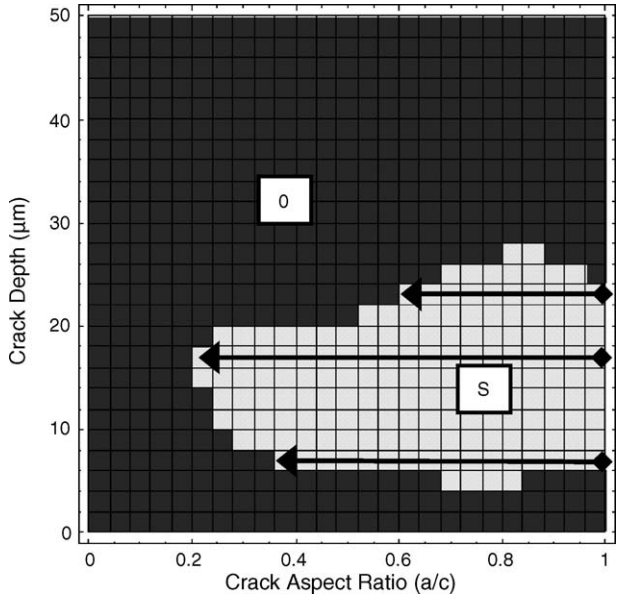

Fig. 7. Crack stability map as a function of crack depth and crack aspect ratio a/c, at an applied stress of 120 MPa. Two-step ion exchanged glass. Black arrows indicate crack growth paths. Conditions for which no crack growth occurs are indicated as (0). Conditions for surface crack growth are indicated as (S).

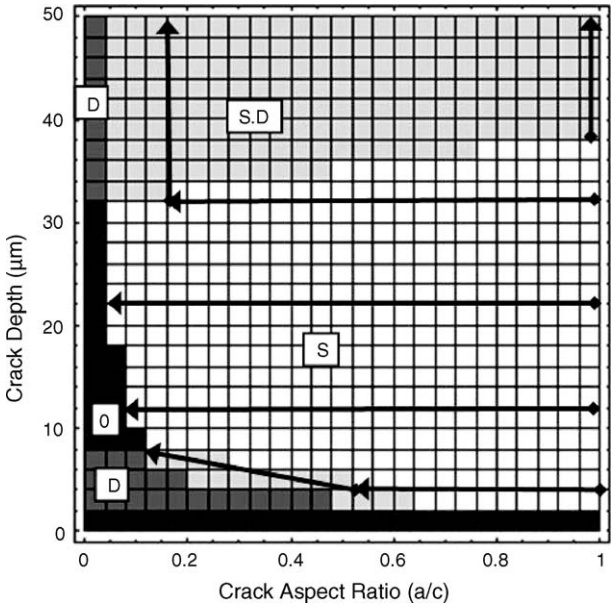

Fig. 8. Crack stability map as a function of crack depth and crack aspect ratio a/c, at an applied stress of 225 MPa. Two-step ion exchanged glass. Black arrows indicate crack growth paths. Conditions for which no crack growth occurs are indicated as (0). Conditions for surface crack growth are indicated as (S). Conditions for depthwise crack growth are indicated as (D).

crack depth and aspect ratio at an applied stress of 120 MPa. According to the graph, semi-circular cracks with depths between 6 and 24 μm in depth will grow across the surface of the material, reaching extended semi-elliptical shapes. Black arrows on the figure show crack growth paths. Fig. 8 shows an analogous graph at an applied stress of 225 MPa. The region of stable surface crack growth has grown. Stable depth wise growth occurs for shallow cracks of 2–8 μm depths, and large cracks above 32 μm depth are predicted to undergo unstable depthwise growth to fracture.

These maps can be combined for a range of applied stresses, resulting in a crack propagation contour map, as shown in Fig. 9. Each black arrow indicates the stable growth path with increasing stress for a crack with a given initial depth and semi-circular geometry. Crack depths are plotted up to 50 μm, encompassing the largest known flaws as calculated from the fracture stress distribution in the untreated material (see Table 1). Overall, cracks are predicted to grow along the surface with increasing stress, until they approach through-thickness geometry. At higher stresses, crack growth occurs in the depth direction until an instability is reached at the predicted fracture stress. The stress contours indicate the extent of stable crack growth at a particular applied stress. For example, at a stress of 100 MPa, flaws between 6 and 14 μm depth are predicted to propagate along the surface and then arrest at the 100 MPa contour line. As stresses increase, cracks continue to propagate along the surface to lower aspect ratios, reaching elongated elliptical or near through-thickness shapes. Note that the predicted final fracture stress for all flaws between 2 and 22 μm is nearly constant. This insensitivity to flaw size is characteristic of ESP glass, and extends well

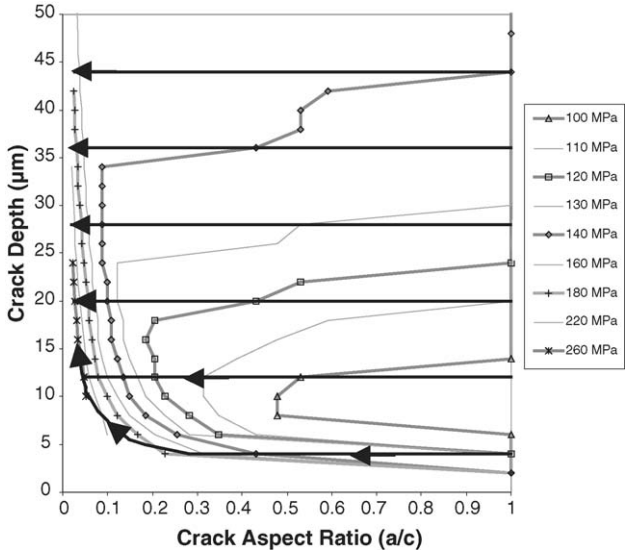

Fig. 9. Predicted crack propagation contour plot for two-step ESP glass, showing critical stresses for crack growth and fracture for a range of initial crack depths. Black arrows indicate paths of stable crack growth with increasing stress, for each initial crack depth.

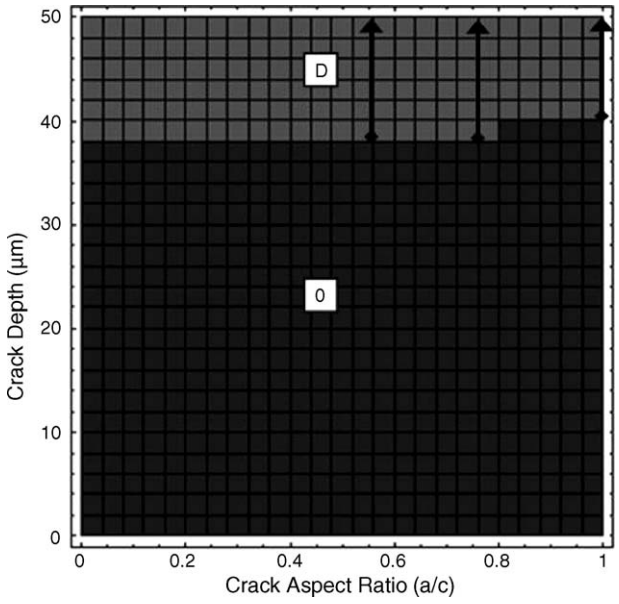

Fig. 10. Single-step ion exchanged glass. Crack stability map as a function of crack depth and crack aspect ratio *a*/*c*, at an applied stress of 225 MPa. Under these conditions, no stable surface crack growth occurs, and large cracks grow unstably to failure. Black arrows indicate crack growth paths. Conditions for which no crack growth occurs are indicated as (0). Conditions for depthwise crack growth are indicated as (D).

beyond the 12–14 μm depth of the maximum compressive stress in the material. The clamping effect of the compressive stress on the walls of the crack increases the required stress for fracture, even beyond the point of maximum compressive stress. This can be seen intuitively in Eq. (2), which integrates the stress profile over the full depth of the crack.

As flaw size increases above 22 μm, fracture strength begins to decrease, but limited stable growth of near through-thickness cracks continues for flaws up to 50 μm in depth. Two distinct types of fracture behavior are thus apparent: stable growth of small flaws resulting in fracture at a fixed stress independent of flaw size, and limited stable growth of large flaws ending in fracture at a range of lower stresses. Stable surface crack growth to low aspect ratios is indicated for cracks well beyond the depth of the maximum compressive stress, an unexpected result not predicted by prior studies. Extremely large or extremely small flaws are expected to bypass the stable growth phase entirely. These flaws do not propagate until they reach the critical stress for unstable fracture, and are affected relatively little by the shape of the residual stress profile. Note that the precision of the crack propagation graph is limited by the number of data points. Finer detail requires considerably greater computation time, but allows more exact prediction.

A similar set of graphs were produced for the single step exchange, and used to predict fracture stresses as a function of flaw size, for both through-thickness and semi-circular flaw geometries. An example is shown in Fig. 10, at the same applied stress as Fig. 8 (225 MPa). In contrast to the graph for the two-step exchange, no region of stable crack growth is present. Contour mapping provided little additional insight in this case.

Table 2 compares predicted and experimental values of onset stress for multiple surface cracking, for a threshold flaw surface length of 100 μm. The experimental onset stress for multiple cracking for the fine surface preparation is slightly higher than either of the other two processes, likely due to the differing flaw size distributions produced by each surface preparation method. The calculation appears to underestimate the onset stress in all cases. One possible reason for the error is the limited number of cracks present in the material. The crack propagation maps assume that cracks of every possible aspect ratio and size are present, and therefore multiple cracking will initiate at the applied stress at which the most favorable flaw is predicted to grow stably. In an actual specimen, such a flaw may not be present, and thus higher stresses are needed to activate flaws that may have slightly non-optimal shape or orientation. The prediction is least accurate for the fine surface finish specimens, which presumably have the fewest large surface flaws. Note that the predicted onset stress takes into account the 100 μm minimum distinguishable threshold length, and thus is higher than the 100 MPa

Table 2
Predicted and experimental onset stresses for stable crack growth in the two-step ion exchanged glass

Surface finish	Predicted onset stress (MPa)	Experimental onset stress[a] (MPa)	Percent error (%)
Coarse	120	139.9 ± 3.4	−14
Medium	120	127.5 ± 1.8	−6
Fine	120	147.1 ± 4.6	−19

[a] ± values represent one standard deviation above and below the mean value.

Table 3
Predicted and experimental fracture strengths of ESP glasses

Surface finish and process	Experimental fracture strength[a] (MPa)	Predicted fracture strength, semi-circular flaws[a] (MPa)	Percent error (%)	Predicted fracture strength, through-thickness flaws[a] (MPa)	Percent error (%)
Single-step exchange					
Coarse	303.4 ± 14.1	286.7 ± 33.3	−5.5	330.7 ± 3.2	+9.0
Medium	324.4 ± 12.3	315.8 ± 28.1	−2.7	334.4 ± 3.7	+3.1
Fine	397.3 ± 45.6	328.1 ± 5.5	−17.4	335.2 ± 3.9	−15.6
Two-step exchange					
Coarse	287.6 ± 13.9	237.9 ± 23.7	−17.3	280 ± 0.0	−2.6
Medium	288.3 ± 5.1	266.3 ± 23.7	−7.6	280 ± 0.0	−2.9
Fine	285.4 ± 8.1	275.6 ± 6.8	−3.4	280 ± 0.0	−1.9

[a] ± values represent one standard deviation above and below the mean value.

theoretical stress to initiate stable crack growth given on the contour map in Fig. 9. Other factors may also play a role. The relatively high temperature and aggressive environment of the ion exchange process may change the character of pre-existing flaws, or preferential ion exchange at crack tips may produce localized residual stresses that hinder later crack growth.

A summary of the fracture strength data is shown in Table 3. The first set of predictions assumes that semi-circular flaws are the major source of failure in the untreated glass. The second set assumes a through-thickness surface scratch or similar flaw geometry. It is likely that the actual flaws present in the untreated glass have a variety of shapes, resulting in strength values between the two sets of predictions listed in the table. Indeed, these two limiting cases bracket (or nearly bracket) the experimental fracture stress in most cases. Note that the through-thickness set of predictions, using shallower calculated crack depths, indicates a single value for the strength of the two-step exchanged glass, regardless of surface finish, since the largest flaws in these cases lie entirely within the region of stable growth. The prediction for these conditions appears highly accurate, within 3% of the experimentally measured strengths for each glass, which likewise show relatively little variation in strength compared to the single step processes. The exception to this general good agreement is the single step ion exchange process using a fine surface finish. Experimental data in this case shows an unusually high strength and a large variation in strength as measured by the standard deviation, a pattern not associated with stable crack growth.

Several factors are not addressed by the prediction method, but could play a role in determining the fracture behavior of the material. The measured stress profile is averaged over the surface of the specimen, and may not be uniform in all areas. Specifically, preferential ion exchange at crack tips during processing would result in an uneven stress profile, and thus affect the fracture stress. The high temperature molten salt environment of the ion exchange baths could also affect the shape of pre-existing flaws, or relax localized residual stresses at flaw sites. Subcritical crack growth has been observed in the propagation of multiple surface cracks in ESP glasses,[11,13] and could reduce onset stresses for stable surface crack growth as well as alter fracture stresses. Interactions between growing cracks could also affect observed strengths.

Crack shielding and crack deflection parallel to the surface have been noted in prior work on ESP soda alumina silica glasses.[9,11,13,18,22] However, these effects are unlikely to play a major role in this study. No crack deflection was noted in the soda lime silica glasses used in the current work. Crack shielding is also unlikely to be significant, due to the observed non-uniformity of the surface crack distribution. At an observed crack spacing of 200 μm, and a calculated crack depth of 10 μm, work by Isida[23] suggests a shielding effect of less than 2%. Although some cracks in close proximity will be shielded, fracture can still occur at unshielded, isolated cracks, yielding no overall increase in strength.

4. Conclusions

It was found that progressively finer surface polishing had little effect on the strength of soda lime silica ESP glass made by two-step ion exchange, while significantly increasing the strength of untreated and single exchange step glasses. The second exchange step in each case reduced the strength of the glass, and decreased the strength variability.

ESP glass surfaces demonstrated multiple cracking behavior under tensile stress. The density of these cracks was found to be variable and inhomogeneous, increasing with applied tensile stress. Cracks appeared initially as localized flaws, and then grew to through-thickness surface cracks with increasing stress. Fine surface polishing reduced the number of propagating surface cracks.

A weight function method was used to predict multiple cracking and fracture stress distributions based on measured residual stress profiles. Stable crack growth and uniform fracture strengths were predicted over a range of flaw depths extending beyond the depth of the maximum compressive stress for the two-step ion exchanged glass. Fracture strength predictions were accurate within 20% for all conditions studied, and within 10% for most cases. Predictions of onset stress for multiple cracking show fair agreement with the experimental data. Errors may be caused by the limited number

and variety of flaws in the test specimens, the geometric limits of the stress intensity factor prediction method, the presence of subcritical crack growth, and possible effects of the ion exchange bath on the flaw population in the material.

Acknowledgements

Financial support was provided by Sandia National Laboratories. Sandia is a multiprogram laboratory operated by Sandia Corporation, a Lockheed Martin Company, for the United States Department of Energy under Contract DE-ACO4-94AL85000.

References

1. Kistler, S. S., Stresses in glass produced by nonuniform exchange of monovalent ions. *J. Am. Ceram. Soc.*, 1962, **45**(2), 59–68.
2. Cooper, A. R. and Krohn, D. A., Strengthening of glass fibers II, ion exchange. *J. Am. Ceram. Soc.*, 1969, **52**(12), 665–669.
3. Bartholomew, R. F. and Garfinkel, H. M., Chapter 6: Chemical strengthening of glass. *Glass Science and Technology, Vol 5: Elasticity and Strength in Glasses*. Academic Press, 1980.
4. Green, D. J. and Maloney, B. R., Influence of surface stress on indentation cracking. *J. Am. Ceram. Soc.*, 1986, **69**(3), 223–225.
5. Tandon, R., Green, D. J. and Cook, R. F., Strength variability in brittle materials with stabilizing and destabilizing resistance fields. *Acta Metall. Mater.*, 1993, **41**(2), 399–408.
6. Schaeffer, H. A., Thermal and chemical strengthening of glass—review and outlook. In *Strength of Inorganic Glass*, ed. C. R. Kurkjian. Plenum Press, 1985, pp. 469–483.
7. Green, D. J., Tandon, R. and Sglavo, V. M., Crack arrest and multiple cracking in glass through the use of designed residual stress profiles. *Science*, 1999, **283**, 1295–1297.
8. Tandon, R. and Green, D. J., The effect of crack growth stability induced by residual compressive stresses on strength variability. *J. Mater. Res.*, 1992, **7**(3), 765–771.
9. Green, D. J., Critical parameters in the processing of engineered stress profile glasses. *J. Non-Cryst. Solids*, 2003, **316**(1), 35–41.
10. Sglavo, V. M., Larentis, L. and Green, D. J., Flaw-insensitive ion-exchanged glass: I, Theoretical aspects. *J. Am. Ceram. Soc.*, 2001, **84**(8), 1827–1831.
11. Sglavo, V. M. and Green, D. J., Flaw-insensitive ion-exchanged glass: II, Production and mechanical performance. *J. Am. Ceram. Soc.*, 2001, **84**(8), 1832–1838.
12. Sglavo, V. M. and Bonafini, M., Design and production of a high reliability soda lime silicate glass. In *Ceramics – Processing, Reliability, Tribology and Wear*, ed. G. Müller. Wiley-VCH, 2000, pp. 353–358.
13. Abrams, M. B., Green, D. J. and Glass, S. J., Fracture behavior of engineered stress profile soda lime silicate glass. *J. Non-Cryst. Solids*, 2003, **321**(1–2), 10–19.
14. Shen, J. and Green, D. J., Variable-temperature ion-exchanged engineered stress profile (ESP) glasses. *J. Am. Ceram. Soc.*, 2003, **86**(11), 1979–1981.
15. Abrams, M. B. and Green, D. J., Prediction of stable crack growth geometry in residually stressed glass. *Int. J. Frac.*, 2004, **130**(2), 601–615.
16. Harper, C. A., *Handbook of Ceramics, Glasses, and Diamonds*. McGraw-Hill, New York, USA, 2001.
17. Abrams, M. B., Shen, J. and Green, D. J., Residual stress measurement in ion-exchanged glass by iterated birefringence and etching. *J. Test. Eval.*, 2004, **32**(3), 1–7.
18. Abrams, M. B., *Crack Propagation and Fracture in Engineered Stress Profile Glass*. Doctoral thesis, The Pennsylvania State University, 2004.
19. Glinka, G. and Shen, G., Universal features of weight functions for cracks in mode I. *Eng. Frac. Mech.*, 1991, **40**(6), 1135–1146.
20. Shen, G. and Glinka, G., Weight functions for a surface semi-elliptical crack in a finite thickness plate. *Theor. Appl. Frac. Mech.*, 1991, **15**, 247–255.
21. Wang, X. and Lambert, S. B., Stress intensity factors for low aspect ratio semi-elliptical surface cracks in finite-thickness plates subjected to nonuniform stresses. *Eng. Frac. Mech.*, 1995, **51**(4), 517–532.
22. Green, D. J., Sglavo, V. M., Beauchamp, E. K. and Glass, S. J., Designing residual stress profiles to produce flaw-tolerant glass. In *Fracture Mechanics of Ceramics*, *Vol 13*, ed. R. C. Bradt. Kluwer Press, 2002.
23. Isida, M., Tension of a half plane containing array cracks, branched cracks and cracks emanating from sharp notches. *Trans. Japan Soc. Mech. Eng.*, 1979, **45**(392), 306–317.
24. Dillinger, L., *Met-Tips 15, Ideas for Metallographic Procedures. Relationship between Grit Size, Mesh Size, and Micron Size*. http://www.leco.org/customersupport/met-tips/met_tip15.pdf, 2002.